Available online at www.sciencedirect.com

SciVerse ScienceDirect

Acta Materialia 61 (2013) 2025–2032

Acta MATERIALIA

www.elsevier.com/locate/actamat

The structure of Cu–Zr glasses using a colloidal proxy system

R.C. Kramb [a,b,*], L.T. Ward [c], K.E. Jensen [d], R.A. Vaia [a], D.B. Miracle [a]

[a] AFRL/RX Materials & Manufacturing Directorate, Air Force Research Laboratory, Wright-Patterson AFB, OH 45433, USA
[b] National Research Council, Washington, DC 20001, USA
[c] Department of Material Science and Engineering, The Ohio State University, Columbus, OH 43210, USA
[d] Department of Physics, Harvard University, Cambridge, MA 02138, USA

Received 17 July 2012; received in revised form 11 December 2012; accepted 18 December 2012
Available online 21 January 2013

Abstract

We present a novel experimental technique for studying the structure of metallic glasses (specifically Cu–Zr) through a proxy system of charged colloidal particles. A dense suspension of two types of colloidal particles that match the relative size ratio and approximate the attractive interaction of Cu and Zr atoms is created. Confocal microscopy images are analyzed to find the location of tens of thousands of particles at each composition studied. The particle locations are used to determine the packing fraction, partial radial distribution functions and partial coordination numbers of each component as well as the shape of clusters (central atom and first shell neighbors) that form. These results are compared to experimental and simulation literature on Cu–Zr systems, with good agreement found among all structural properties.

Keywords: Metallic glasses; Colloidal glasses; Amorphous materials; Glass structure

1. Introduction

Despite their discovery more than 50 years ago [1], many questions remain about the structure of metallic glasses. Even for the simplest case of a binary system (e.g. Cu–Zr), structure-predicting theories rarely are able to successfully define a structure beyond the first neighbor shell [2]. Scattering experiments performed on actual metallic glass samples give useful structural information but also have drawbacks. Because the scattering experiments result in structural information that is averaged over the relatively large area of the beam, single-atom resolution is not possible. Furthermore, as more components are added and the complexity of the system is increased, more experiments are needed to resolve the contributions from each component. For example, with two components (e.g. Cu–Zr), three experiments are needed to resolve the Cu–Cu, Zr–Zr and Cu–Zr partial distribution functions, and six independent diffraction experiments are needed to separate the partial distribution functions in a ternary glass. The ability to bypass these difficulties would greatly enhance the ability to study the structure of metallic glasses, but the number of independent diffraction experiments needed to resolve the constituent particles is a fundamental limitation. Significant progress is being made in spatial resolution, but the techniques are challenging to employ, the equipment is highly specialized and interpretation of the results is still evolving.

Historically, two strategies have been implemented to tackle these obstacles. The first is to run classical or ab initio molecular dynamics (MD) simulations that attempt to replicate the solidification of a few thousand atoms. While simulations allow for the tracking of each atom in the system, they are limited by computing capacity to a small volume which may not be statistically sufficient. A typical simulation run includes a volume of $\sim$10 nm^3 and represents an elapsed time on the order of a few picoseconds,

* Corresponding author at: AFRL/RX Materials & Manufacturing Directorate, Air Force Research Laboratory, Wright-Patterson AFB, OH 45433, USA.
E-mail address: ryan.kramb.ctr@wpafb.af.mil (R.C. Kramb).

1359-6454/$36.00 © 2012 Acta Materialia Inc. Published by Elsevier Ltd. All rights reserved.
http://dx.doi.org/10.1016/j.actamat.2012.12.022

which does not match well with the length and timescales of actual lab processes. The second approach is to use physical spheres that create a proxy to stand in for the actual atoms in order to scale up their size so that they can be seen in real space. This approach has successfully been used as far back as 1960, when steel ball bearings were used to study the structure of monodispersed spheres [3]. More recently, Lee and coworkers used a binary mixture of steel ball bearings where the relative size of the balls matched that of Cu and Zr atoms, but the interaction between them was simply that of volume exclusion [4]. Now, with the development of confocal microscopy and particle tracking codes, colloidal particles can be used as a proxy for many atomic scale systems [5]. In this case, particles are suspended in a solvent with the same index of refraction so that the suspension appears translucent and does not scatter light. A fluorescent dye is incorporated into either the solvent or the particles and, with the use of a confocal microscope, a three-dimensional (3-D) image stack can be created showing the location of many particles within the sample volume. Most of the work using colloids and confocal microscopy so far has been limited to monodispersed particles and/or hard sphere interactions [6–10], which have limited applicability for studying metallic glasses with atomic interactions. In this paper, we present a new colloidal system that, by including attractive forces, more closely reproduces the interatomic forces found in real metallic glasses compared to simple hard sphere-like interactions. We use a binary mixture of two sizes of colloidal particles (radius ratio = 0.78) where one type of particle is positively charged and one type is negatively charged. The result is a net attraction between unlike particles and a net repulsion between like particles, which more closely matches the interaction of Cu and Zr than simple hard spheres and results in significantly better agreement with measured structural properties of real Cu–Zr than previous proxy systems. We examine structural features including partial radial distribution functions, partial coordination numbers and Voronoi indices of structurally important 12- and 10-fold clusters from samples with compositions ranging from the Cu–Zr equivalents of $Cu_{43}Zr_{57}$ to $Cu_{83}Zr_{17}$. The best glass forming compositions for real Cu–Zr glasses are found near $Cu_{60}Zr_{40}$ and we cover a range of ~±20% from this point in both directions. We also compare the results from charged particles with uncharged particles to explore the structural differences that result from different particle potentials.

2. Experimental

2.1. Particle synthesis

The core colloid particles are made using the emulsion polymerization technique, and unless otherwise noted, synthesis reagents are purchased from Sigma–Aldrich and used as-received. A typical reaction goes as follows and is primarily based on the techniques developed in Ref. [11]. In a 500 ml round bottom flask, 270–290 ml of methanol is mixed with 10–30 ml of either deionized water or formamide, bringing the total volume to 300 ml. 12 g of polyvinylpryolidone (PVP, K30 molecular weight) is then dissolved in the solution to act as a stabilizer for the growing particles. Next, 11.7 ml of methylmethacrylate monomer, 18.3 ml 2,2,2 trifluoroethylmethacrylate monomer and 1.5 ml of 2-(2-bromoisobutyryloxy)ethyl methacrylate inimer (initiator + monomer) is added. Finally, 0.3 g of azobisisobutyronitrile (AIBN) is added and the flask is sealed with a rubber stopper. A continuous stream of nitrogen is blown into the flask through a syringe needle (with a second needle providing an outlet) and the flask is moved to a silicon oil bath on a hot plate set to 55 °C and stirred with a magnetic stir bar at 700 rpm. The reaction proceeds for 18 h, after which the stopper is removed, stopping the reaction. The resulting particles are monodispersed spheres with a size from ~1 μm to 4 μm, depending on the amount of water/formamide used in the reaction [12]. The particles are cleaned by repeated centrifugation and resuspension cycles, first in 1:1 water–methanol then in pure water. For this work, we use particles with mean diameters of 2.9 μm and 3.7 μm. The smaller particles are proxies for Cu atoms and the larger particles represent Zr atoms.

2.2. Surface charge

The surface of the particles contain a reactive Br-inimer species that allows a polymer to be grown using a technique called surface initiated atom transfer radical polymerization (SI-ATRP). This technique uses a copper catalyst to grow a polymer outward from the inimer sites, and can be used with many different types of polymers. For this work, we grow a negatively charged acrylamide on the Cu particles and a positively charged acrylamide on the Zr particles. The typical SI-ATRP reaction for negatively [positively] charged particles is as follows. After the unmodified particles have been cleaned, they are suspended in 4 ml of water at 50% particles by volume (8 ml total volume) and transferred to a 100 ml round bottom flask. 8.5 ml of water and 14 ml of formamide is added to the flask. 2 ml of N,N-dimethylacrylamide (DMAM), 0.5 ml of 2-acrylamido-2-methyl-1-propanesulfonic acid sodium salt solution, 50% in water (AM-acid) [(3-acrylamidopropyl)trimethylammonium chloride solution, 75% in water (AM-Cl)] and 0.165 ml of 1,1,4,7,10,10-hexamethyltriethylenetetramine is then added. Next, 10 mg of Cu(II)Cl is added and nitrogen is bubbled through the solution for 30 min. Finally, 50 mg of Cu(I)Cl is added, the flask is capped with a stopper and nitrogen is streamed in with a pair of needles. The reaction is stirred at 400 rpm and proceeds at room temperature for 2 h until the stopper is removed. The relative amount of AM-acid [AM-Cl] to DMAM can be changed to increase or decrease the resulting surface charge and the reaction time can be adjusted as well.

Because light scattering techniques are used to resolve surface potentials and subsequently particle interaction potentials, it is difficult to fully describe the interaction between particles in the index-matched solvent needed for confocal microscopy. Instead, we measure the zeta potential in deionized (DI) water using a Malvern Zeta-Sizer DLS instrument and approximate the interaction qualitatively. Typical surface functionalization reactions result in zeta potentials between −10 mV and −50 mV [+10 mV and +50 mV] in DI water. The particles used in this work have a zeta potential of +33 mV and −47 mV for Cu and Zr particles, respectively. Using the relative magnitude of these potentials and the general shape of electrostatic interactions we can predict the qualitative shape of the three types of interactions present, as shown in Fig. 1. The charged particles are then cleaned by centrifugation and resuspended in water.

2.3. Fluorescent labeling

The particles are labeled with two fluorescent dyes, one for the positively charged particles and one for the negatively charged particles. To do this, 1.75 mg of either Pyrromethene 546 (blue) or 605 (red) compound (Exciton, Inc.) is dissolved in 1.75 ml of toluene. At the same time, 70 mg of Brij 58 surfactant is dissolved in 7 ml of DI water. After dissolution, these two solutions are mixed with a tip sonicator for 2 min, resulting in an opaque emulsion. The dye emulsion is added to 70 ml of the particle/water suspension and capped with a stopper. The dye suspension is stirred for at least 24 h with a magnetic stir bar at room temperature. The suspension is moved to a hot plate at 55 °C, the stopper is removed and a weak stream of nitrogen is blown over the surface of the suspension. The flask is stirred at 400 rpm for 5 h and small amounts of DI water are added every 30 min to maintain the liquid level. This process slowly evaporates the toluene while leaving the dye trapped inside the particles. At the end of 5 h, the particles are again cleaned by centrifugation in 1:1 water–methanol, and then water only.

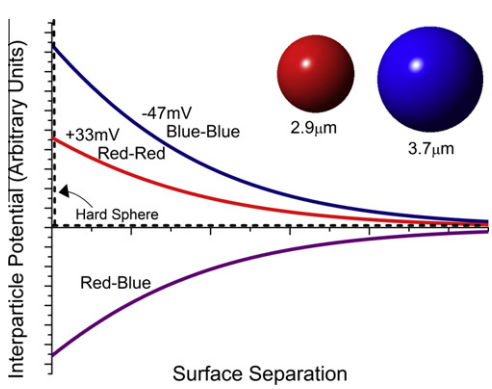

Fig. 1. Qualitative potential energy for Cu–Cu interactions (red), Zr–Zr interactions (blue) and Cu–Zr interaction (purple). Also shown is a simple hard sphere interaction as a dashed line. (For interpretation of the references to color in this figure legend, the reader is referred to the web version of this article.)

2.4. Sample preparation

This process gives negatively charged particles dyed "red" from Pyrromethene 605 with an effective diameter of 2.9 μm, and positively charged particles dyed "blue" from Pyrromethene 546 with an effective diameter of 3.7 μm. A small amount of each particle suspension is transferred from the centrifuge tube into a small vial such that the composition of the final sample is controlled by the volume of each particle suspension added. The vial is then dropped into a tube and centrifugation is used to replace the water in the suspension with formamide, which has the same refractive index as the combination of polymers used to synthesize the core particles. The result is a translucent orange-colored suspension which is then transferred to a small, 12.5 mm diameter cylinder made from copper pipe with a circular No. 1 microscope cover slip adhered to one end with epoxy. The copper cylinder sample cell is then dropped into a centrifuge tube, cover slip down, and spun a final time at 5000 rpm for 20 min. The excess formamide is poured off, leaving a dense particle suspension at the bottom. The total volume of the sample is ~1 ml, of which ~70% is particle volume and 30% is remaining solvent.

2.5. Imaging and analysis

The sample cell is flipped, cover slip side up, and image stacks are acquired with a Zeiss LSM700 model confocal laser scanning microscope. A 63 × oil immersion objective is used to scan an area ~100 × 100 μm in the X–Y plane for each slice. Each Z-direction step is 0.2 μm, resulting in ~500 images and $100 \times 100 \times 100\ \mu m^3$ total volume, which includes on the order of 10^5 particles. The images are loaded into Matlab and the location of each of the two types of particles is found using routines based on the particle finding code developed by Maria Kilfoil and coworkers [13]. The accuracy of the locating code was checked by visual inspection by comparing tagged particles such as those in Fig. 2c and d with the original images such as the image in Fig. 2b. Missing or double-counted particles were found to be less than 1% of the total. The error in locating the center of particles of comparable size using this method was calculated to be on the order of 0.01 μm, less than 1% the total diameter of these particles. With the location of each particle recorded, the software calculates the partial radial distribution functions (PRDFs) for each component. A different Matlab package uses the Voro++ code [14] to find nearest neighbors of each particle with the Voronoi tessellation method and to analyze the composition and shape of nearest neighbor clusters. Fig. 2 shows an example of the images used in the analysis for a composition of $Red_{53}Blue_{47}$ ($Cu_{53}Zr_{47}$).

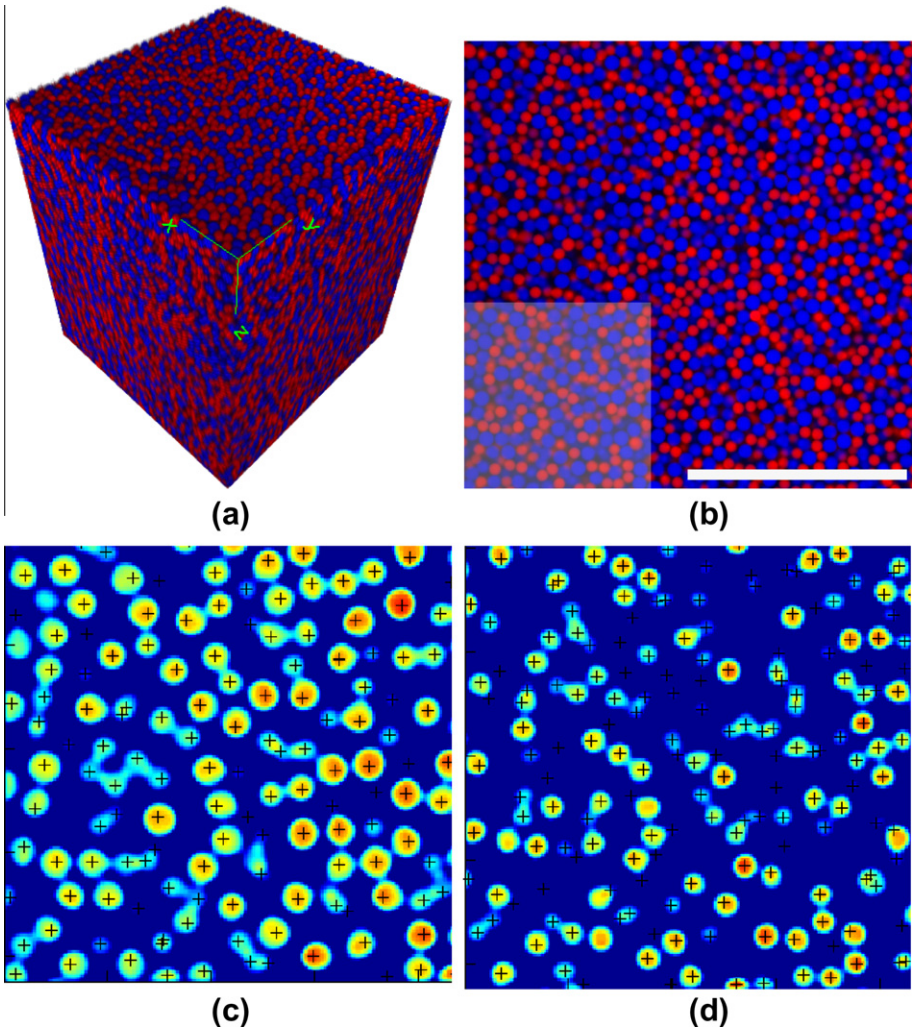

Fig. 2. (a) 3-D rendering of confocal image stack volume where Cu-proxy particles are red and Zr-proxy particles are blue. (b) One slice taken from the middle of the stack. The scale bar represents 50 μm. (c) Blue particles identified in gray section of the slice using Matlab code and marked with "+". (d) Red particles identified and marked. (For interpretation of the references to color in this figure legend, the reader is referred to the web version of this article.)

Preliminary analysis of the image stacks was done in increments of 50 images to determine the number of particles in each 10 μm segment of the stack. This allowed us to determine if the composition in the sample was consistent throughout as well as to determine if the number density of particles remained constant as the images move away from the cover slip. In Fig. 3, we show the results from two samples at the same overall composition of Red_{70}-$Blue_{30}$ ($Cu_{70}Zr_{30}$). Dashed curves show a sample with Red particles that do not have the negatively charged polymer on the surface so there is no attractive force between the Red and Blue particles. The result is a gradient in the composition throughout the sample where there are few Blue particles near the cover slip and more as one moves away (blue curve, left axis). The solid curves show the results from a sample where Red particles are negatively charged and Blue particles are positively charged. Here the composition remains constant at 30% Blue throughout. However, the total number of particles (purple curves,

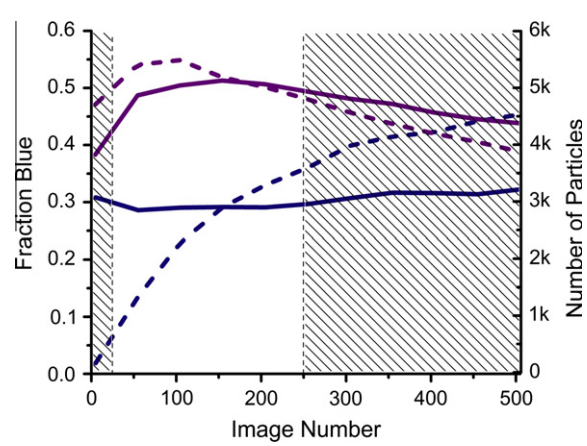

Fig. 3. Variation in composition (blue, left axis) and number of particles (purple, right axis) per 50 image segment through a sample with an overall composition of $Red_{70}Blue_{30}$ ($Cu_{70}Zr_{30}$). Dashed curves are for non-interacting particles with no charge on Red particles. Solid curves are for attractive particles due to negative charge on Red and positive charge on Blue. (For interpretation of the references to color in this figure legend, the reader is referred to the web version of this article.)

right axis), and therefore the packing fraction, falls as one moves away from the coverslip and into the sample. The particle density remains relatively constant up to approximately image 250. The initial increase in the number of particles for images 0–50 is due to the fact that the first few images are taken before reaching the centers of any particles, i.e. below the cover slip. Finally, we note that approximately the first four to eight layers of particles retain some degree of crystallization due to the flat coverslip. Because of these points, the rest of the discussion will focus primarily on samples using oppositely charged particles and only images from 25 to 250, as indicated from the shaded areas of Fig. 3. Deviations from these two criteria will be noted.

3. Results and discussion

The main panel of Fig. 4 shows the PRDFs for a Red_{56}-$Blue_{44}$ ($Cu_{56}Zr_{44}$) sample with oppositely charged particles, while the inset shows the same $Red_{70}Blue_{30}$ ($Cu_{70}Zr_{30}$) sample as in Fig. 3. The red, blue and purple curves are for Red–Red (Cu–Cu), Blue–Blue (Zr–Zr) and Red–Blue (Cu–Zr) respectively. The structure from this PRDF is clearly not crystallized and is qualitatively consistent with previous experimental and simulation work for Cu–Zr glasses [15,16]. The locations of the first peaks at 2.9 μm and 3.7 μm give the effective size of Red and Blue particles, which results in a relative size ratio of 0.78:1. This is close to the desired ratio of 0.80:1 that is the generally accepted value for the ratio of Cu and Zr atomic sizes. The mixed Red–Blue peak is higher than either of the other two peaks, indicating the preference for forming unlike bonds between Red and Blue particles. This is in agreement with recent simulation work on Cu–Zr glasses [15]. In the main panel the second peaks for the Red–Red and Red–Blue curves appear to be splitting, indicating some degree of medium range order (MRO). This has been seen in Cu–Zr simulation work where a system is cooled from a liquid phase with no MRO to a glass phase with MRO [15]. As with previous Cu–Zr work, splitting of the Blue–Blue (Zr–Zr) second peak is much less noticeable. Although there is considerable uncertainty in the exact location of these second peaks, their positions relative to the first peak position compares favorably to those reported in Ref. [15]. In our data the Red–Red second peaks are slightly closer together at 1.85 and 1.94σ1, while for Duan et al. [15], the positions are 1.75 and 2.03σ1, where σ_1 is the position of the first peak. The second peak splitting is not apparent in the inset figure, which also agrees with Cu–Zr metallic glass literature in that $Cu_{56}Zr_{44}$ is a better glass forming composition than $Cu_{70}Zr_{30}$ [17]. Also in the inset of Fig. 4 with dashed curves, is the PRDF for the non-interacting particle sample at an overall composition of $Red_{70}Blue_{30}$. Here, the Red–Blue peak height is greatly reduced, indicating the absence of a driving force for forming unlike bonds.

Using the locations of the centers of mass of each particle, we draw a three-dimensional Voronoi tessellation around each particle that encloses all points closest to that particle. The tessellation is drawn using the "radical" Voronoi approach, which ensures that for mixtures of different particle sizes, no edge or face of a tessellation cuts through a neighboring particle by weighting the separation distance of the dividing plane on the size of the particle [14]. By comparing the volume of each Voronoi cell with the volume of each particle (calculated as the volume of a sphere with the diameter equal to the location of the first peak in the PRDF), we can estimate the local packing fraction (ϕ) for each particle. The distribution of ϕ is shown in Fig. 5 for $Red_{56}Blue_{44}$ ($Cu_{56}Zr_{44}$). Here we see that the packing around larger Blue particles is more efficient than around the smaller Red particles. This is expected due to the geometrical packing of different sized spheres, since there is less empty space when small spheres surround a large sphere than when large spheres surround a small sphere. However, as shown in a later section, the smaller Red par-

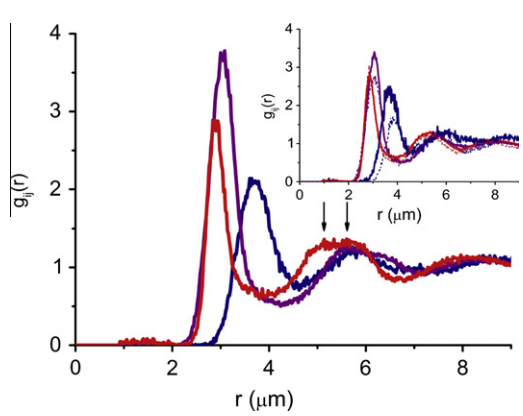

Fig. 4. Main panel: partial radial distribution function of a single sample at a composition of $Cu_{56}Zr_{44}$. The double arrows indicate the locations of the split second peaks for Cu–Cu. Inset: PRDF for composition of $Red_{70}Blue_{30}$ ($Cu_{70}Zr_{30}$) for charged particles (solid) and neutral particles (dashed). (For interpretation of the references to color in this figure legend, the reader is referred to the web version of this article.)

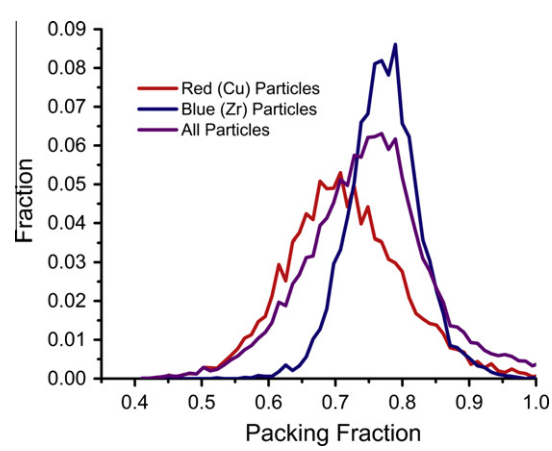

Fig. 5. Distribution of packing fractions calculated by comparing spherical particle volumes to volume of Voronoi cells around each particle, from a single sample with a composition of $Red_{56}Blue_{44}$ ($Cu_{56}Zr_{44}$). (For interpretation of the references to color in this figure legend, the reader is referred to the web version of this article.)

ticles are actually closer to having the theoretical maximum number of neighbors when the size differences are taken into account. The peak for all particles is found at $\phi \sim 0.75$, which is higher than is reported for Cu–Zr metallic glasses [18] (using density measurements and reported atomic sizes, the packing fraction varies from ~0.73 to 0.74 depending on composition) and likely means that the particles are actually slightly smaller than is indicated by the position of the first peak in the PRDF. Packing fraction distributions at different compositions are qualitatively similar and do not show any significant trend. We also examine packing in terms of particle number density. The volume of the imaged section of the sample is $100 \times 100 \times 45$ μm, and the total number of particles within this volume gives the number density. In Fig. 6, we compare these number densities, normalized by the volume of a Red particle, with experimental values [18] that are normalized by the volume of a Cu atom.

Using the Voronoi cells to define first shell neighbors as those that share a Voronoi face allows us to calculate a distribution of partial and total coordination numbers rather than a single value (as is done when using PRDF to calculate coordination numbers). In Fig. 7, we show the distribution of coordination numbers for $Red_{56}Blue_{44}$ ($Cu_{56}Zr_{44}$) with the constraint that the shared Voronoi face must be at least 1% of the total area of the Voronoi cell, and the maximum separation distance for first shell neighbors is defined by the position of the first minimum in the PRDF curve for each sample. For $Red_{56}Blue_{44}$ ($Cu_{56}Zr_{44}$), we see that the most common number of neighbors around Red-centered clusters is 11, found in more than 18% of all clusters (33% of Red-centered clusters). Red-centered clusters range from having as little as 6 (0.01%) to as many as 15 (0.07%) neighbors. The most common coordination number for Blue-centered clusters is 14 with 15 only slightly less common. These account for 12% and 11% of

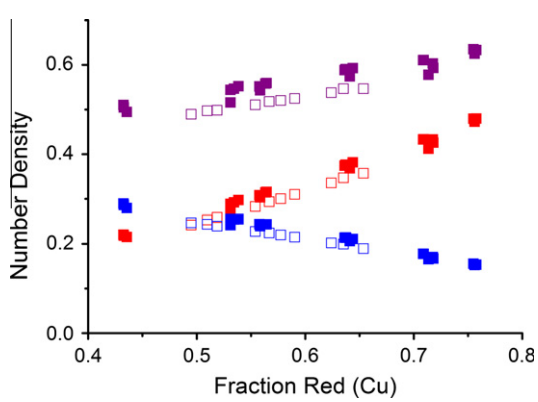

Fig. 6. Calculated number densities of Red (red), Blue (blue) and Total (purple) particles as a function of Red particle composition (solid points). Number densities for Cu (red), Zr (blue) and Total (purple) atoms as a function of Cu composition (open points). Density is reported as a fraction of red particle or Cu atom volume. (For interpretation of the references to color in this figure legend, the reader is referred to the web version of this article.)

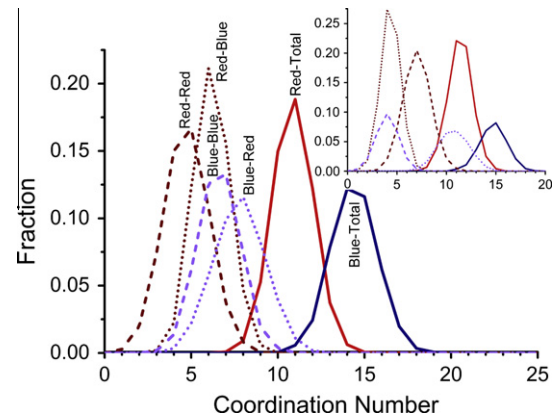

Fig. 7. Distribution of partial and total coordination numbers from a single sample with a composition of $Red_{56}Blue_{44}$ ($Cu_{56}Zr_{44}$) with the y-axis representing the fraction of all clusters. The first color above each distribution is the center particle, while the second is the type of particle in the first neighbor shell. Inset: distribution of coordination numbers for $Red_{70}Blue_{30}$ ($Cu_{70}Zr_{30}$). (For interpretation of the references to color in this figure legend, the reader is referred to the web version of this article.)

all clusters (28%, 27% of Blue-centered cluster). There are, however, Blue-centered clusters with as few as nine (0.01%) and as many as 19 (0.07%) neighbors. We can also examine the components that make up these clusters. For Red-centered clusters, the most common cluster is made with 6 Blue (solid, dark red curve) and 5 Red particles (dashed, dark red curve) in the first coordination shell giving a total cluster composition of six Red and six Blue particles. For Blue-centered clusters, the most common has eight Red (solid, blue-green curve) and seven Blue for a total composition of eight Red and eight Blue. For the $Red_{70}Blue_{30}$ ($Cu_{70}Zr_{30}$) composition shown in the inset, there are more Red particles in the system and the number of Red neighbors has increased for both central particle types, while the total number of neighbors has not significantly changed with the most common Red centered cluster still having 11 neighbors and the most common Blue cluster now having 15.

The mean partial and total coordination numbers are calculated from the distributions and are shown in Fig. 8 for Red centered clusters and Fig. 9 for Blue centered clusters. In both figures, solid red data points are for Red neighbors, solid blue data points are Blue neighbors and solid purple data points are total neighbors. Also included in Figs. 8 and 9 are experimental and simulation results from Refs. [16,17] with circles representing experimental data from Mattern et al. and diamonds representing simulation data from Ma et al. The agreement is near quantitative, with Mattern et al. finding slightly fewer Blue (Zr) neighbors and slightly more Red (Cu) neighbors for Red (Cu) centered clusters. For all three sets of data, the number of total first shell neighbors for Red (Cu) centered clusters rises from ~10 at a composition of $Red_{40}Blue_{60}$ ($Cu_{40}Zr_{60}$) to ~12 for $Red_{80}Blue_{20}$ ($Cu_{80}Zr_{20}$). For Blue (Zr) centered clusters in Fig. 8, the results are very similar, with Mattern et al. finding fewer Red (Cu) neighbors, and

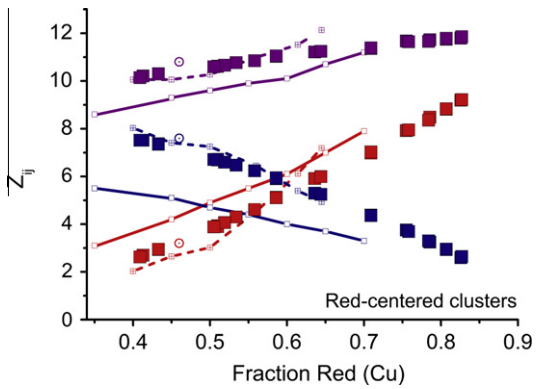

Fig. 8. Mean coordination numbers for Red (Cu) centered clusters with Red–Red (Cu–Cu) in red, Red–Blue (Cu–Zr) in blue and Red–Total (Cu–Total) in purple. Data from this work calculated from Voronoi analysis is in filled symbols. Comparison to Ref. [16] are open squares, and comparison to Ref. [17] are + squares. The three circle points at Red fraction = 0.46 are from MD simulations of $Cu_{46}Zr_{54}$ in Ref. [15]. (For interpretation of the references to color in this figure legend, the reader is referred to the web version of this article.)

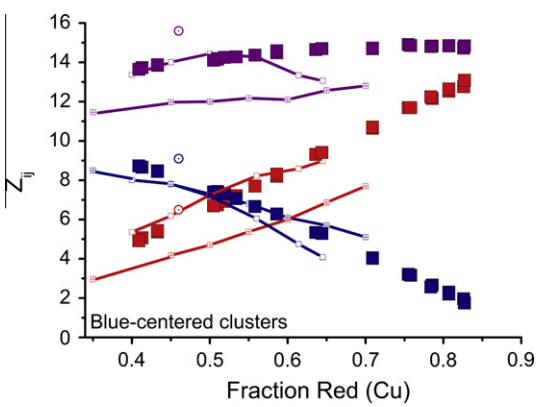

Fig. 9. Mean coordination numbers for Blue (Zr) centered clusters with Blue–Red (Zr–Cu) in red, Blue–Blue (Zr–Zr) in blue and Blue–Total (Zr–Total) in purple. Data from this work calculated from Voronoi analysis is in closed points. Comparisons to X-ray diffraction experiments from Refs. [16,17] are open squares, and + squares respectively, and comparisons to MD simulations from Ref. [15] are filled circles. (For interpretation of the references to color in this figure legend, the reader is referred to the web version of this article.)

quantitative agreement within experimental error with the results from Ma et al. Here the total number of neighbors rises from just over 13 at $Red_{40}Blue_{60}$ ($Cu_{40}Zr_{60}$) to a plateau of ~15 for $Red_{75}Blue_{25}$ ($Cu_{75}Zr_{25}$). For higher concentrations of Red (Cu), the total coordination around Blue (Zr) particles falls slightly. The experimental data have an assessed error of ±1 [19].

The Cu–Zr system has a significant negative heat of mixing that produces six binary intermetallic compounds. This shows a clear preference to form bonds between unlike atoms and suggests that chemical short-range ordering should be present. However, the mean partial coordination numbers in Fig. 7 give no obvious indication of chemical ordering. This agrees with earlier experimental and computational results [15–17], which show that the degree of chemical short-range order is within experimental error of complete disorder. In fact, the observed trends [17] suggest that the most stable glasses have the smallest degree of chemical order. There is at present no clear explanation for this unexpected behavior.

To describe how efficiently packed the clusters are and using arguments from Ref. [20], Ma et al. showed that in actual Cu–Zr glasses, Cu centered clusters came closer to the theoretical maximum coordination number for spheres of their relative size [17]. In Fig. 10, we compare our data (solid points) to theirs (open points). In the figure, the color of the data points represents the central particle with red for Cu and blue for Zr. The *y*-axis is the number of Zr neighbors in the first shell, while the *x*-axis is the number of Cu neighbors. For a cluster containing only the same type of particle as the center, it can be shown that 13.3 is the maximum coordination number. For clusters with Cu sized spheres at the center and only Zr spheres in the first shell, 10.1 is the maximum. For Zr centers and only Cu in the first shell, 16.9 is the maximum. By assuming a linear relationship between the extremes, we can plot mixed coordination numbers with the theoretical maximum. We find that Red (Cu) centered clusters tend to fall closer to the theoretical line than Blue (Zr) clusters, in agreement with Ma et al. This indicates that first shell of Red (Cu) centered clusters is near the efficient packing limit and suggests that Red (Cu) clusters are the primary structural units. The insets show a ten-vertex Cu cluster with two Cu and eight Zr in the first shell and a 12-vertex icosahedron with eight Cu and four Zr in the first shell which would be found at the arrow points.

Finally, in addition to the composition of first shell clusters, we can also determine their exact shape. For example,

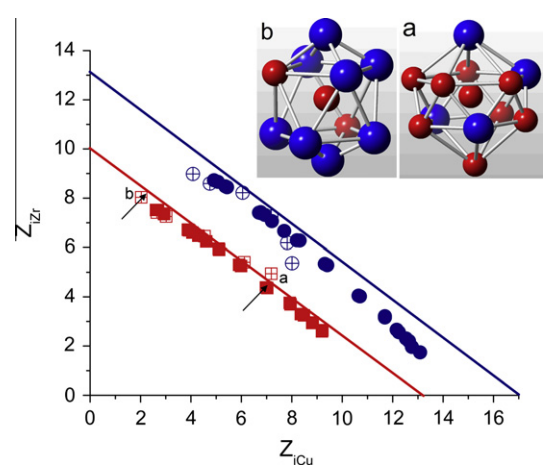

Fig. 10. Distance from theoretical maximum coordination number for Cu (red) and Zr (blue) and compared to Ref. [17] (open symbols). The inset represents Red-centered (or Cu-centered) clusters with Voronoi indices of $\langle 0,0,12,0\rangle$ and $\langle 0,2,8,0\rangle$ that would be found at points a and b respectively as found in Ref. [17]. (For interpretation of the references to color in this figure legend, the reader is referred to the web version of this article.)

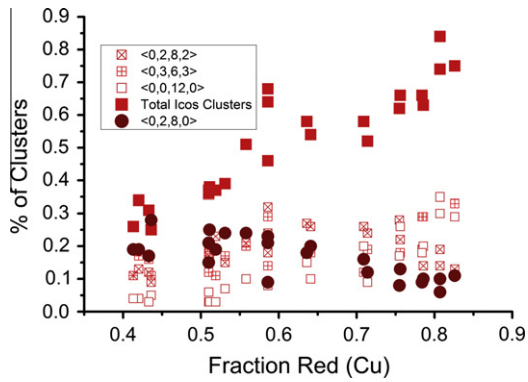

Fig. 11. Fraction of clusters that are icosahedron-like (Voronoi indices of $\langle 0,2,8,2\rangle$, $\langle 0,3,6,3\rangle$ or $\langle 0,0,12,0\rangle$) in red squares and those that are 10-sided prism (Voronoi index of $\langle 0,2,8,0\rangle$) in darker red circles.

clusters containing 12 neighbors can form an icosahedron shape that tends to be a very stable configuration and high numbers of icosahedra often indicate good glass formability. We analyze cluster shapes using the four-number Voronoi index. Here an index of $\langle 0,0,12,0\rangle$ indicates a perfect icosahedron shape, while $\langle 0,2,8,2\rangle$ and $\langle 0,3,6,3\rangle$ are 12-sided distorted icosahedra. In Fig. 11, we plot the percentage of all clusters that have these three indices as well as a ten-sided prism shape with an index of $\langle 0,2,8,0\rangle$. The fraction of icosahedral clusters generally increases with more Cu particles and there appears to be a local maximum near $Cu_{58}Zr_{42}$ although there is some scatter in the data. This is in qualitative agreement with simulations of Cu–Zr [21]. The fraction of ten-sided prism clusters generally decreases with increasing Cu concentrations.

4. Conclusion

We have demonstrated that colloidal particles can be an excellent proxy for atomic systems when certain key parameters are tuned correctly. For the Cu–Zr metallic glass system chosen here, we designed the colloid system to have the same relative size ratio as Cu–Zr atoms and an interaction such that unlike particles feel an attractive force. By incorporating a fluorescent dye molecule into the particle cores, we imaged the suspension using confocal microscopy techniques and obtain the location of the centers of tens of thousands of particles. In a single image stack, we obtained partial radial distribution functions, and partial coordination numbers that match the atomic system of interest. But by using the colloidal proxy system, we also obtained information that is usually only possibly with simulations. For example, we calculated the coordination number of every particle in the system using Voronoi cell analysis and generated distribution of coordination numbers rather than a single value for the entire sample. We compared the packing efficiency of individual particles as well, through the calculation of Voronoi cell volumes. Finally, we examined the shapes of clusters that make up the structure using the Voronoi indices of the clusters. Each of these structural metrics for the colloidal system compared favorably to both experiments and simulations with Cu–Zr metallic glasses. Therefore, we have shown that a properly designed colloidal system provides a valid and useful proxy for studying metallic glass structure. In addition to the correct radius ratios, we have shown that attractive forces are also necessary for designing a suitable proxy system. Without the electrostatic charges on the surface of the particles, so that the particles behave like hard spheres, the composition varied throughout the sample, and details of the structure did not match as well with metallic glass experiments and simulation.

Acknowledgements

The authors thank Tom Kodger for discussions on particle synthesis, surface charge and solvent choice. We also thank David Weitz and Frans Spaepen for discussion and access to their resources. Work at the Air Force Research Laboratory was supported through the Air Force Office of Scientific Research and under on-site Contract No. F49620-02-C-0015 conducted through the National Research Council, Washington, DC.

References

[1] Klement W, Willens RH, Duwez POL. Nature 1960;187:869.
[2] Miracle DB. Nat Mater 2004;3:697.
[3] Bernal JD. Nature 1960;185:68.
[4] Lee J-C, Park K-W, Kim K-H, Fleury E, Lee B-J, Wakeda M, et al. J Mater Res 2007;22:3087.
[5] Prasad V, Semwogerere D, Eric RW. J Phys: Condens Matter 2007;19:113102.
[6] Schall P, Cohen I, Weitz DA, Spaepen F. Science 2004;30:1944.
[7] Schall P, Weitz DA, Spaepen F. Science 2007;318:1895.
[8] Lynch JM, Cianci GC, Weeks ER. Phys Rev E 2008;78:031410.
[9] Narumi T, Franklin SV, Desmond KW, Tokuyama M, Weeks ER. Soft Matter 2011;7:1472.
[10] Eisenmann C, Kim C, Mattsson J, Weitz DA. Phys Rev Lett 2010;104:035502.
[11] Russell ER, Sprakel J, Kodger TE, Weitz DA. Soft Matter 2012;8:8697.
[12] Lindstrom SB, Kodger TE, Sprakel J, Weitz DA. Soft Matter 2012;8:3657.
[13] Gao Y, Kilfoil ML. Opt Exp 2009;17:4685.
[14] Rycroft CH. Voro++: Chaos 2009;19:041111.
[15] Duan G, Xu D, Zhang Q, Zhang G, Cagin T, Johnson WL, et al. Phys Rev B 2005;71:224208.
[16] Mattern N, Schops A, Kuhn U, Acker J, Khvostikova O, Eckert J. J Non-Crystal Solids 2008;354:1054.
[17] Ma D, Stoica AD, Wang XL, Lu ZP, Xu M, Kramer M. Phys Rev B 2009;80:014202.
[18] Li Y, Guo Q, Kalb JA, Thompson CV. Science 2008;322:1816.
[19] Miracle DB, Laws KJ, Senkov ON, Wilks GB. Metall Mater Trans 2012:1002.
[20] Miracle DB, Sanders WS, Senkov ON. Philos Mag 2003;83:2409.
[21] Sha ZD, Feng YP, Li Y. Appl Phys Lett 2010;96:061903.